The oral hypoxia-inducible factor prolyl hydroxylase inhibitor enarodustat counteracts alterations in renal energy metabolism in the early stages of diabetic kidney disease

see commentary on page 855

OPEN

Sho Hasegawa[1,2], Tetsuhiro Tanaka[1], Tomoyuki Saito[3], Kenji Fukui[1,3], Takeshi Wakashima[1,3], Etsuo A. Susaki[4,5], Hiroki R. Ueda[4,5,6] and Masaomi Nangaku[1]

[1]Division of Nephrology and Endocrinology, The University of Tokyo Graduate School of Medicine, Tokyo, Japan; [2]Research Fellowship for Young Scientists, Japan Society for the Promotion of Science, Tokyo, Japan; [3]Biological and Pharmacological Research Laboratories, Central Pharmaceutical Research Institute, Japan Tobacco Inc., Takatsuki, Japan; [4]Department of Systems Pharmacology, The University of Tokyo Graduate School of Medicine, Tokyo, Japan; [5]Laboratory for Synthetic Biology, RIKEN Center for Biosystems Dynamics Research, Suita, Japan; and [6]WPI International Research Center for Neurointelligence, The University of Tokyo Institutes for Advanced Study (UTIAS), The University of Tokyo, Tokyo, Japan

Hypoxia-inducible factor (HIF) prolyl hydroxylase inhibitors, also known as HIF stabilizers, increase endogenous erythropoietin production and serve as novel therapeutic agents against anemia in chronic kidney disease. HIF induces the expression of various genes related to energy metabolism as an adaptive response to hypoxia. However, it remains obscure how the metabolic reprogramming in renal tissue by HIF stabilization affects the pathophysiology of kidney diseases. Previous studies suggest that systemic metabolic disorders such as hyperglycemia and dyslipidemia cause alterations of renal metabolism, leading to renal dysfunction including diabetic kidney disease. Here, we analyze the effects of enarodustat (JTZ-951), an oral HIF stabilizer, on renal energy metabolism in the early stages of diabetic kidney disease, using streptozotocin-induced diabetic rats and alloxan-induced diabetic mice. Transcriptome analysis revealed that enarodustat counteracts the alterations in diabetic renal metabolism. Transcriptome analysis showed that fatty acid and amino acid metabolisms were upregulated in diabetic renal tissue and downregulated by enarodustat, whereas glucose metabolism was upregulated. These symmetric changes were confirmed by metabolome analysis. Whereas glycolysis and tricarboxylic acid cycle metabolites were accumulated and amino acids reduced in renal tissue of diabetic animals, these metabolic disturbances were mitigated by enarodustat. Furthermore, enarodustat increased the glutathione to glutathione disulfide ratio and relieved oxidative stress in renal tissue of diabetic animals. Thus, HIF stabilization counteracts alterations in renal energy metabolism occurring in incipient diabetic kidney disease.

Correspondence: *Tetsuhiro Tanaka or Masaomi Nangaku, 7-3-1 Hongo, Bunkyo-ku, Tokyo 113-8655, Japan. E-mail: tetsu-tky@umin.ac.jp or mnangaku-tky@umin.ac.jp*

Received 15 May 2019; revised 11 November 2019; accepted 5 December 2019; published online 25 December 2019

Kidney International (2020) **97,** 934–950; https://doi.org/10.1016/j.kint.2019.12.007

KEYWORDS: diabetic kidney disease; energy metabolism; hypoxia-inducible factor 1; metabolome; prolyl hydroxylase inhibitors; transcriptome

Translational Statement

Hypoxia-inducible factor (HIF) prolyl hydroxylase inhibitors (also known as HIF stabilizers) increase endogenous erythropoietin production and serve as novel therapeutic agents against anemia in chronic kidney disease. Our transcriptome and metabolome analyses of renal tissue in rat and mouse diabetic models have revealed that enarodustat (JTZ-951), an oral HIF stabilizer, counteracts renal energy metabolism alterations in the early stages of diabetic kidney disease. The results provide important data for extrapolating the effects of HIF stabilizers on renal energy metabolism in clinical settings, although further studies are needed to clarify how this renal metabolism reprogramming by HIF stabilizers affects the progression of diabetic kidney disease.

Hypoxia-inducible factor (HIF) prolyl hydroxylase inhibitors increase endogenous erythropoietin production and serve as novel therapeutic agents against anemia in chronic kidney disease.[1]

Cells are endowed with a defensive mechanism against hypoxia, and HIF is a master regulator of this defense.[2,3] Kidneys are physiologically exposed to hypoxia, and chronic hypoxia is recognized as a final common pathway leading to end-stage kidney disease.[4,5] Considering that HIF induces the expression of various genes related to hypoxia responses, HIF stabilizers might have pleiotropic effects on the progression of kidney

diseases as well as improvement in anemia in chronic kidney disease. Interestingly, HIF induces the expression of glycolytic genes and pyruvate dehydrogenase kinase 1, which inhibits pyruvate dehydrogenase from using pyruvate to fuel the mitochondrial tricarboxylic acid (TCA) cycle.[6,7] This metabolic reprogramming from TCA cycle to glycolysis represses oxygen consumption and is critical for adaptation of cells exposed to hypoxic environments. However, it remains obscure how the metabolic reprogramming of renal tissue by HIF stabilization affects the pathophysiology of kidney diseases.

Diabetic kidney disease (DKD) is the major cause of end-stage kidney disease.[8] Systemic metabolic disorders such as hyperglycemia and dyslipidemia cause renal metabolism alterations, leading to renal dysfunction including DKD.[9] Previous studies have shown increased metabolic flux and accumulation of glucose and TCA cycle metabolites in diabetic renal cortical tissue,[10,11] which might be related to mitochondrial dysfunction and DKD progression.[12] We hypothesized that HIF stabilizers might reverse the metabolism alterations in diabetic renal cortical tissue, considering that HIF, as an adaptive response to hypoxia, reduces metabolic flux in cells to repress oxygen consumption. Thus, utilizing transcriptome and metabolome analyses, we conducted a proof-of-concept study to comprehensively understand how enarodustat (JTZ-951),[13,14] an oral HIF stabilizer, affects renal metabolism alterations occurring in the early stages of DKD.

RESULTS

Enarodustat induces metabolic reprogramming from TCA cycle to glycolysis in renal proximal tubule cells

As renal cortex is mainly composed of proximal tubules, we first examined the effects of enarodustat on the metabolic flux of renal proximal tubule cells *in vitro*. First, Mito Stress Test (Agilent Technologies, Inc., Santa Clara, CA) and Glycolytic Rate Assay (Agilent) were conducted in cultured HK-2 cells,[15] a human proximal tubule epithelial cell line (Figure 1a). Enarodustat significantly reduced mitochondrial respiration (TCA cycle) and increased basal glycolysis, indicating metabolic reprogramming from TCA cycle to glycolysis (Figure 1; Supplementary Figure S1). We also conducted an experiment using small interfering RNA (siRNA) for HIF-1 (Figure 2; Supplementary Figure S2). HIF-1 knockdown by siRNA reversed metabolic alterations (basal respiration, maximal respiration, spare respiratory capacity, and adenosine triphosphate [ATP] production) induced by enarodustat, which showed that the metabolic reprogramming was mainly through HIF-1 stabilization (Figure 2; Supplementary Figure S2). Pyruvate dehydrogenase activity, an important factor for cells to use pyruvate to fuel TCA cycle, was also reduced by enarodustat (Figure 2f), which was compatible with the previously published observations.[6,7]

Background data of streptozotocin-induced diabetic rats

From the results of *in vitro* experiments, we hypothesized that HIF stabilizers might alleviate metabolism alterations in diabetic renal cortical tissue through metabolic reprogramming from TCA cycle to glycolysis. We first chose streptozotocin (STZ)-induced diabetic rats as the model for the proof-of-concept experiment to test the above-mentioned hypothesis. In this model, diabetes is rapidly induced, allowing us to observe the net effects of diabetes and HIF stabilizers on the energy metabolism in renal tissue within a short period of time.

The study protocol and basic data from experiments in STZ-induced diabetic rats are shown in Figure 3a. We divided the rats into 3 groups: group A (sham), group B (DKD), and group C (DKD + enarodustat). Blood plasma glucose, glycosylated hemoglobin HbA_{1c}, triglyceride, and total cholesterol levels on day 14 were significantly increased in diabetic groups as compared with group A, whereas there were no significant differences between groups B and C (Figure 3d–g). Although plasma creatinine levels were not different between groups, urinary albumin excretion was significantly increased and glomerulomegaly was noticeable in group B as compared with group A, and enarodustat tended to reverse these changes (Figure 4). Blood urea nitrogen levels were higher in diabetic groups, reflecting dehydration due to diabetes. In summary, the kidneys of STZ-treated rats in our study represent the early stages of DKD. Transcriptome and metabolome analyses were conducted using renal cortical tissue of these rats.

Transcriptome analysis of renal cortical tissue

The results of transcriptome analysis of renal cortical tissue are shown in Figures 5 and 6. Principal component analysis and hierarchical clustering analysis indicated that groups A, B, and C were separated into different clusters, respectively (Figure 5a and b). Differentially expressed genes were selected by $|\log_2$ fold-change (FC)$| \geq 0.5$ and Q value < 0.05. Gene ontology and canonical pathway analyses revealed that genes related to fatty-acid metabolism were upregulated in group B compared with group A. In contrast, genes related to glucose metabolism and hypoxia response including HIF-1 network were upregulated in group C compared with group B (Figure 5c and d).

We also conducted gene set enrichment analysis (GSEA) using the transcriptomics data (Figure 6, Tables 1 and 2). Gene sets of fatty-acid and amino-acid metabolism were upregulated in group B compared with group A (Figure 6). In contrast, these gene sets were downregulated, and gene sets of glucose metabolism were upregulated in group C as compared with group B, showing that enarodustat reversed metabolism alterations induced by diabetes (Figure 6). Moreover, gene sets of TCA cycle were downregulated in group C compared with group B (Table 2), which is compatible with the notion of enarodustat-induced metabolic reprogramming in proximal tubules observed in our *in vitro* study. In summary, enarodustat counteracted diabetic renal metabolism alterations from transcriptomic perspectives.

Metabolome analysis of renal cortical tissue

We measured the absolute concentrations of 116 energy-related metabolites in renal cortical tissue of rats ($n = 4$, for each group) randomly selected from each group (Supplementary Table S1; Supplementary Figure S3). Partial

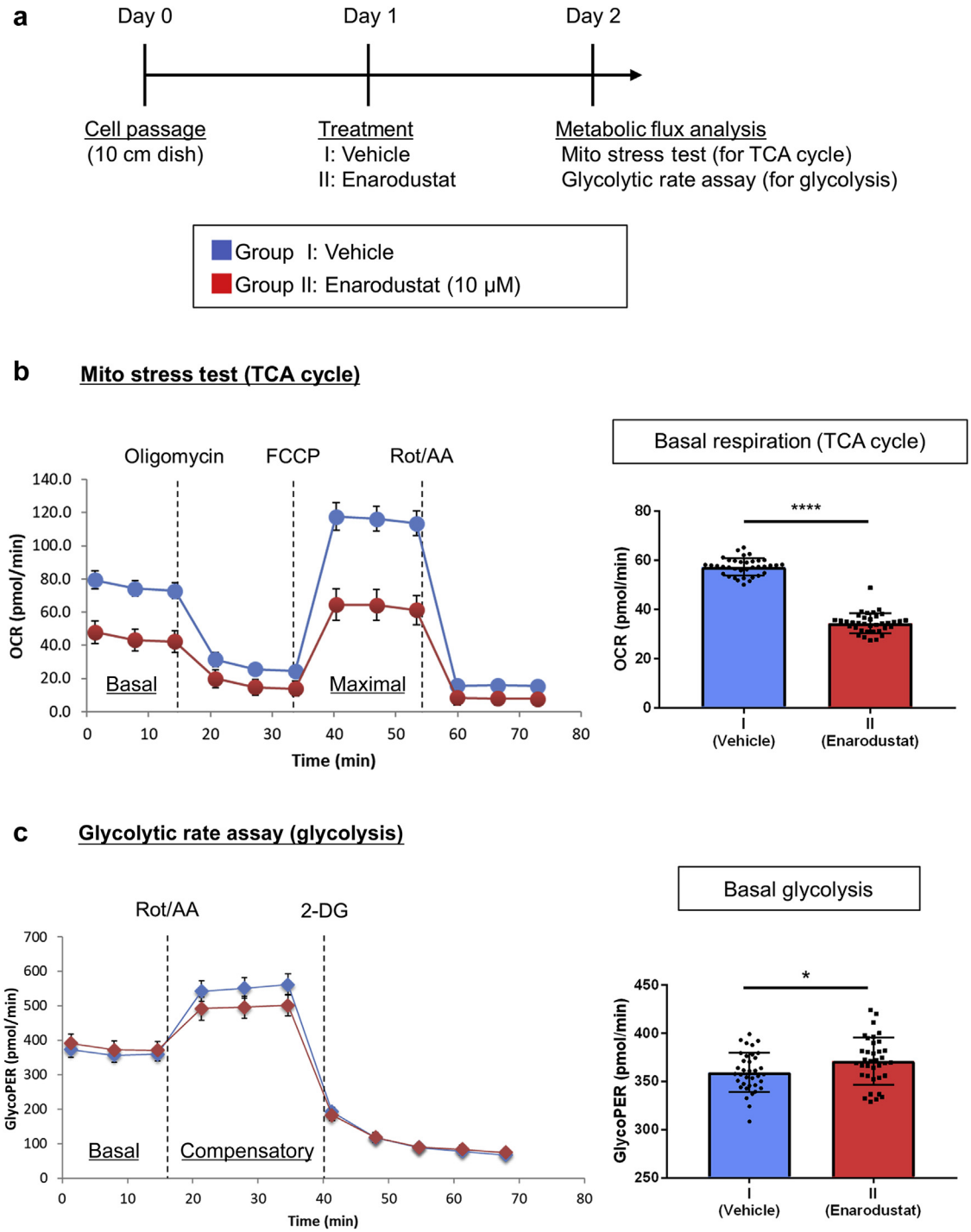

Figure 1 | Enarodustat induces metabolic reprogramming from tricarboxylic acid (TCA) cycle to glycolysis in renal proximal tubule cells. (**a**) Study protocols are shown. (**b**) Mito Stress Test: O_2 consumption rates (OCR) were measured in real time under basal conditions and in response to indicated mitochondrial inhibitors (oligomycin, carbonyl cyanide-p-trifluoromethoxyphenylhydrazone [FCCP], and rotenone + antimycin A [Rot/AA]). The result of basal respiration (TCA cycle) is shown ($n = 36$ for each group, ****$P < 0.0001$). (**c**) Glycolytic Rate Assay: Glycolytic proton efflux rate was measured in real time under basal conditions and in response to Rot/AA (mitochondrial inhibitors) and 2-deoxy-D-glucose (2-DG, a glycolysis inhibitor). The result of basal glycolysis is shown ($n = 36$ for each group, *$P < 0.05$). All data are expressed as mean ± SD. Other parameters including spare respiration capacity and compensatory glycolysis are shown in Supplementary Figure S1. μM, μmol/l.

least squares discriminant analysis (PLS-DA) was performed to assess the significance of class discrimination (Figure 7). We conducted metabolite set enrichment analysis (MSEA) using the metabolites with PLS-DA variable importance in projection (VIP) score ≥ 1. Differences in metabolism of amino acids, such as glycine, serine, methionine, aspartate,

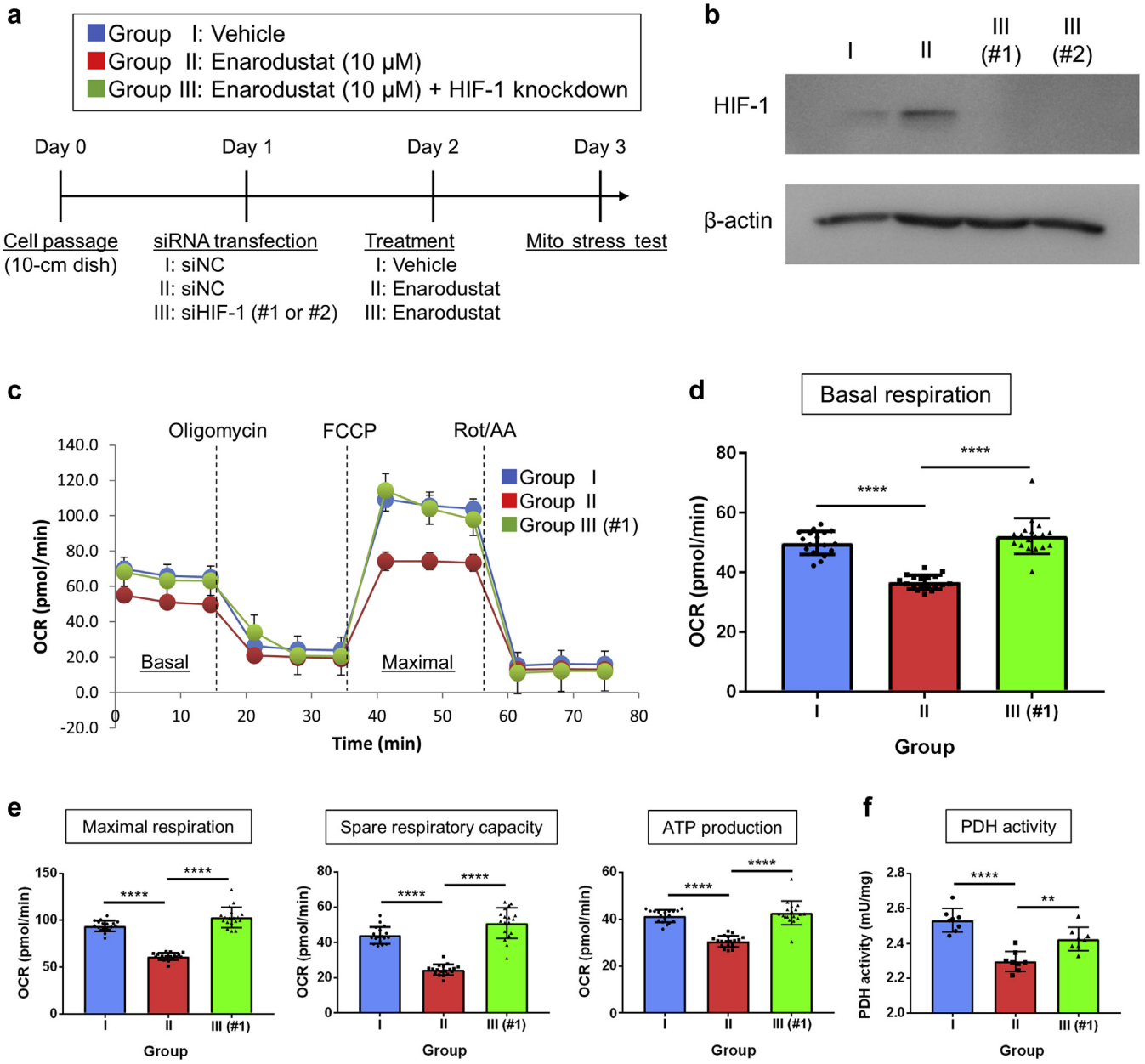

Figure 2 | Metabolic reprogramming by enarodustat occurs mainly through hypoxia-inducible factor-1 (HIF-1) stabilization. (**a**) Study protocols are shown. (**b**) Western blotting for HIF-1 protein at the time of the Mito Stress Test is shown. HIF-1 stabilization induced by enarodustat was successfully reversed by 2 types of small, interfering HIF-1 (siHIF-1; #1 and #2). (**c**) O_2 consumption rates (OCR) were measured in real time under basal conditions and in response to indicated mitochondrial inhibitors (oligomycin, carbonyl cyanide-p-trifluoromethoxyphenylhydrazone [FCCP], and rotenone + antimycin A [Rot/AA]). (**d,e**) HIF-1 knockdown reversed the OCR (basal respiration, maximal respiration, spare respiratory capacity, and adenosine triphosphate [ATP] production) decrease induced by enarodustat ($n = 18$ for each group, $^{****}P < 0.0001$). The experiments using another siHIF-1 (#2) showed the same result (see Supplementary Figure S2). (**f**) Pyruvate dehydrogenase (PDH) activities of these cells are shown. Enarodustat significantly reduced PDH activity through HIF-1 stabilization ($n = 8$, $^{**}P < 0.01$, $^{****}P < 0.0001$). All data are expressed as mean ± SD. μM, μmol/l; siNC, siRNA negative control. To optimize viewing of this image, please see the online version of this article at www.kidney-international.org.

glutamate, arginine, proline, and β-alanine between groups A and B were noted. Differences in amino-acid metabolism were also observed between groups B and C. Moreover, glucose metabolism processes, such as glycolysis and gluconeogenesis, showed different trends between groups B and C (Figure 7).

Visualization of transcriptome and metabolome data on the energy metabolic pathway map

We visualized transcriptome and metabolome data for comprehensive understanding of energy metabolism alterations (Figure 8). Glycolysis and TCA cycle metabolites were found to be accumulated in group B compared with

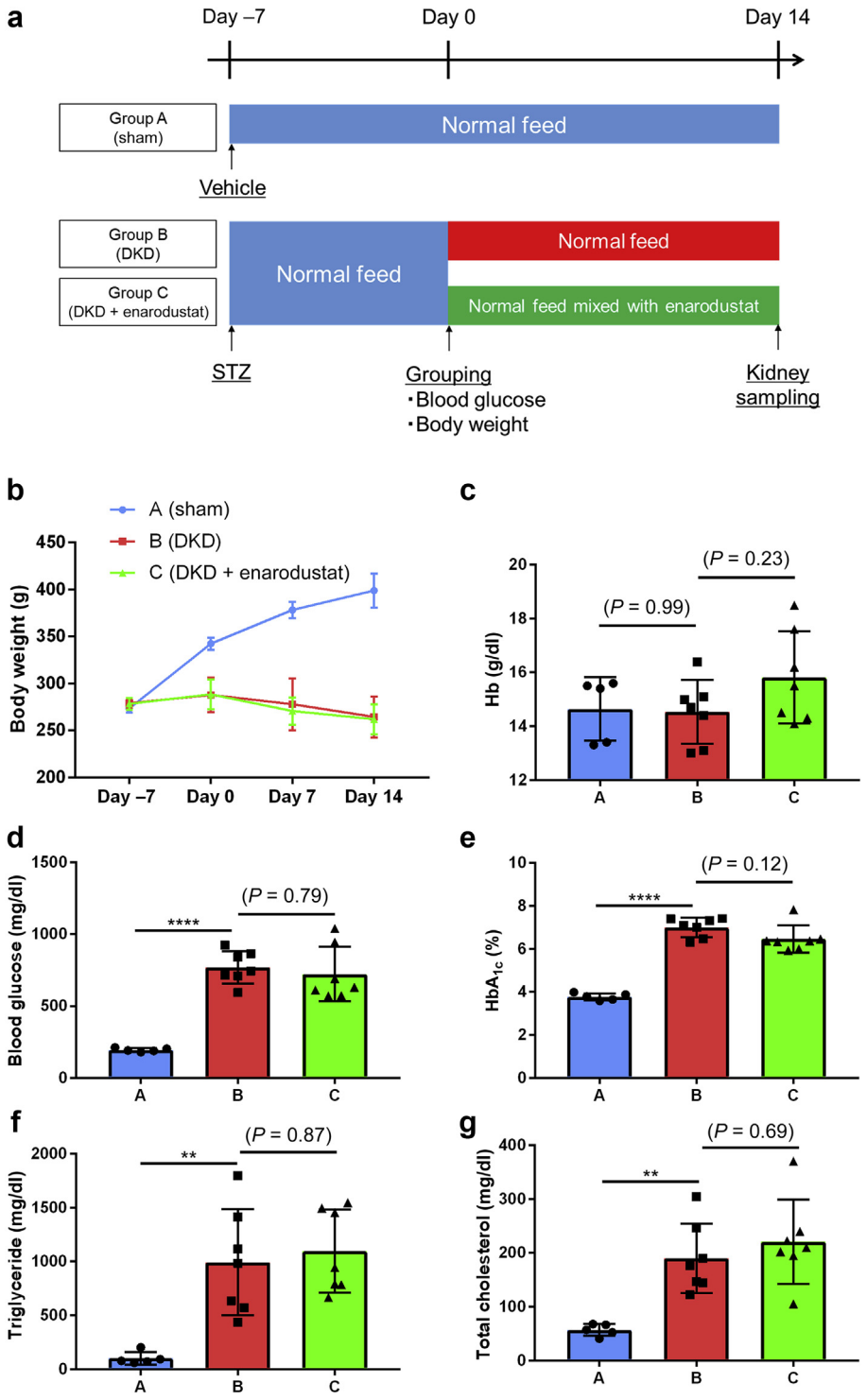

Figure 3 | Study protocols and basic data of streptozotocin (STZ)-induced diabetic rats. (**a**) Study protocols of streptozotocin-induced diabetic rat experiments are shown. (**b**) Transition of the body weights are shown. Body weights were not significantly different between group B (diabetic kidney disease [DKD]) and group C (DKD + enarodustat). (**c**) Hemoglobin (Hb) levels, (**d**) blood glucose levels, (**e**) glycosylated hemoglobin HbA_{1c} levels, (**f**) triglyceride levels, and (**g**) total cholesterol levels on day 14 are shown. For multiplex comparisons, 1-way analysis of variance was applied, followed by the Tukey multiple comparisons test, if appropriate (**$P < 0.01$, ****$P < 0.0001$). All data are expressed as mean ± SD.

group A, which might be due to the excessive glucose inflow and upregulation of fatty-acid metabolism in DKD. Amino acid concentration was reduced in group B compared with group A, reflecting the upregulation of amino-acid metabolism (Figure 8a). In contrast, the accumulation of glycolysis metabolites was relieved by

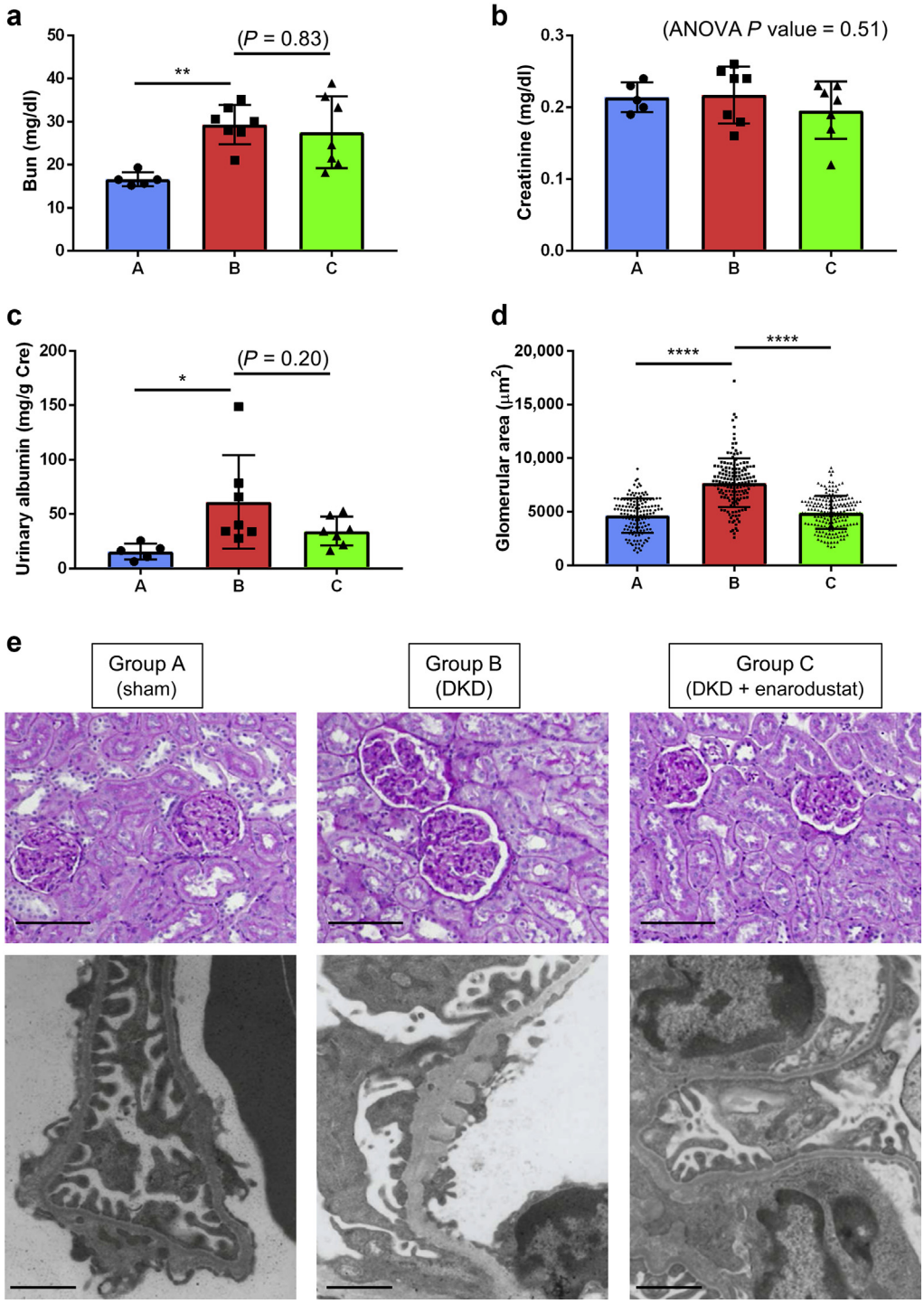

Figure 4 | Basic renal parameters and pathologies in streptozotocin-induced diabetic rats. (**a**) Blood urea nitrogen (BUN), (**b**) plasma creatinine (Cre), and (**c**) urinary albumin levels on day 14 are shown. (**d**) The glomerular area measured in pathological images was markedly increased in group B, and enarodustat reversed this increase (see the periodic acid–Schiff staining images). (**e**) Representative pathological images are shown. (Upper) Periodic acid–Schiff staining images. Bar = 100 μm. (Lower) Electron microscopy images. Glomerular basement membrane thickening was noticeable in group B. Bar = 1 μm. All data are expressed as mean ± SD. For multiplex comparisons, 1-way analysis of variance was applied, followed by the Tukey multiple comparisons test, if appropriate (*$P < 0.05$, **$P < 0.01$, ****$P < 0.0001$). To optimize viewing of this image, please see the online version of this article at www.kidney-international.org.

enarodustat, due to the facilitated flow of glycolysis. Enarodustat also reversed diabetes-induced changes in TCA cycle metabolites and amino acids (Figure 8b). Moreover, enarodustat alleviated the accumulation of glutathione disulfide (GSSG) in diabetic renal tissue and thus showed higher glutathione/GSSG ratio, which suggested that

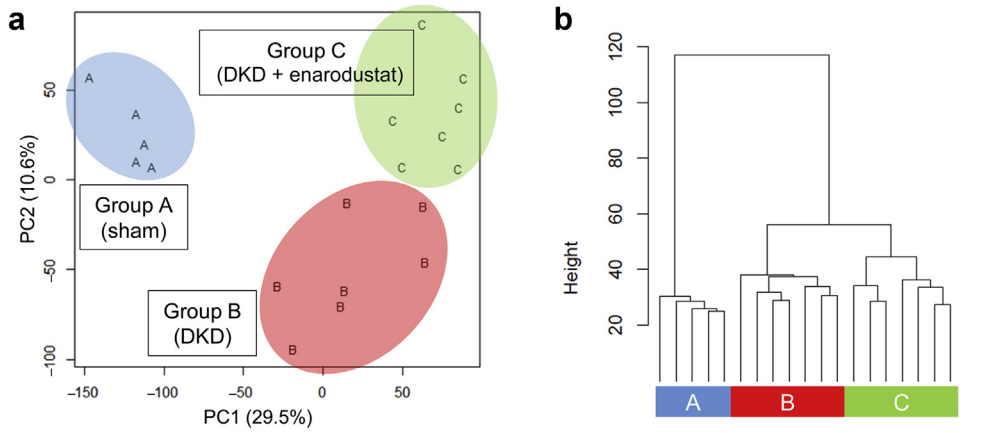

c

Group B (DKD)/A (sham)

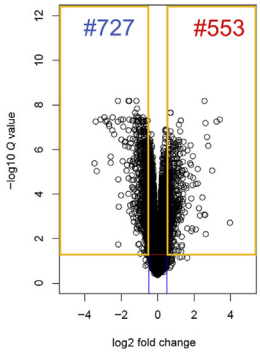

Gene ontology (GO) analysis (top 5)

GO terms	Common genes	Direction	$-Log_{10}$ (*P* value)
Response to nutrient levels	40	up	26.4
Fatty acid metabolic process	25	up	19.9
Response to nutrient	28	up	18.9
Lipid catabolic process	22	up	18.6
Response to organic cyclic compound	28	up	17.8

Canonical pathway analysis (top 5)

Canonical pathways	Common genes	Direction	$-Log_{10}$ (*P* value)
Genes involved in metabolism of lipids and lipoproteins	33	up	20.1
PPAR signaling pathway	16	up	19.4
Fatty acid metabolism	11	up	15.1
Genes involved in fatty acid, triacylglycerol and ketone body metabolism	17	up	13.1
Complement and coagulation cascades	11	up	11.6

Fatty acid metabolism is upregulated by diabetes.

d

Group C (DKD + enarodustat)/B (DKD)

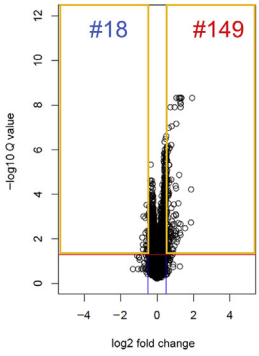

Gene ontology (GO) analysis (top 5)

GO terms	Common genes	Direction	$-Log_{10}$ (*P* value)
Immune response	13	up	11.8
Response to hypoxia	12	up	11.7
Response to decreased oxygen levels	12	up	11.7
Carbohydrate catabolic process	7	up	9.4
Monosaccharide metabolic process	8	up	8.9

Canonical pathway analysis (top 5)

Canonical pathways	Common genes	Direction	$-Log_{10}$ (*P* value)
HIF-1-alpha transcription factor network	9	up	13.7
Glycolysis/gluconeogenesis	8	up	12.4
Genes involved in glycolysis	6	up	10.8
Genes involved in glucose metabolism	7	up	10.2
Genes involved in metabolism of carbohydrates	9	up	9.0

Glucose metabolism is upregulated by enarodustat.

Figure 5 | Transcriptome analysis of renal cortical tissue in streptozotocin-induced diabetic rats. (**a**) Principal component (PC) analysis scores plot and (**b**) hierarchical clustering analysis show that groups A (sham), B (diabetic kidney disease [DKD]), and C (DKD + enarodustat) are separated to respectively different clusters. (**c**) Gene ontology (GO) and canonical pathway analysis of differentially expressed genes (DEGs) in group B/A; DEGs were selected by $|\log_2$ fold-change (FC)$| \geq 0.5$ and Q value < 0.05 (1280 probes; 844 genes). Pathways related to energy metabolism are highlighted in red. (**d**) GO and canonical pathway analysis of DEGs in group C/B; DEGs were selected as described (167 probes; 114 genes). Pathways related to energy metabolism are highlighted in red. Pathways related to hypoxia response are highlighted in green. HIF-1, hypoxia-inducible factor 1; PPAR, peroxisome proliferator–activated receptor.

enarodustat relieved oxidative stress in DKD (Figure 8a and b). The reduction in oxidative stress was confirmed by the levels of the lipid peroxidation marker malondialdehyde in renal cortical tissue: enarodustat reversed the accumulation of malondialdehyde in diabetic renal cortical tissue (Supplementary Figure S4). In summary, integration of

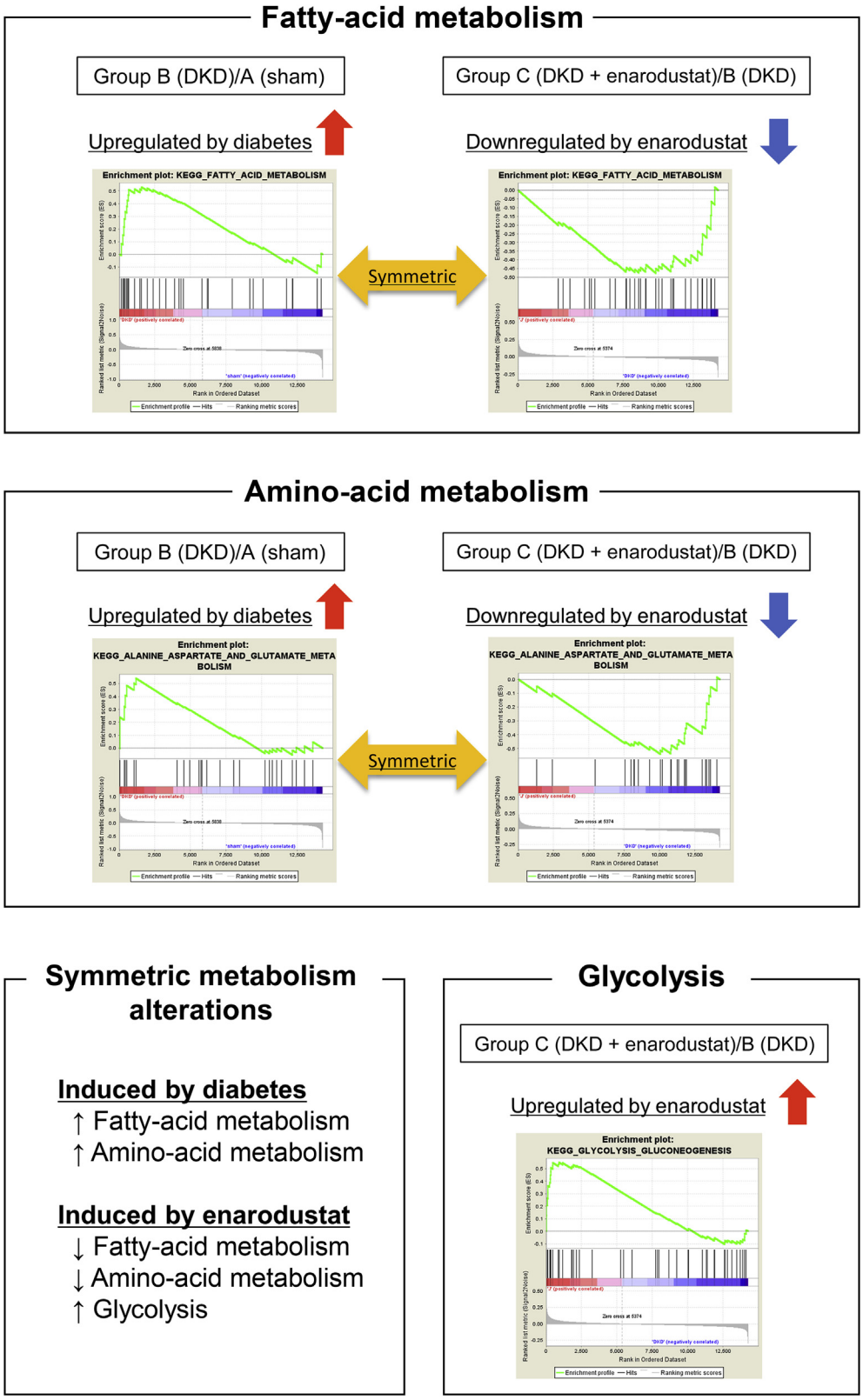

Figure 6 | Gene set enrichment analysis (GSEA) using the transcriptome data. GSEA revealed symmetric metabolism alterations (diabetes vs. enarodustat): fatty-acid and amino-acid metabolisms were upregulated in group B (diabetic kidney disease [DKD]) compared with group A (sham). In contrast, they were downregulated, and glycolysis was upregulated in group C (DKD + enarodustat) compared with group B. Detailed results of GSEA are shown in Tables 1 and 2.

Table 1 | Results of GSEA in group B (DKD)/A (sham)

KEGG canonical pathway (FDR < 0.25)		
Gene sets	NES	-Log$_{10}$ (FDR)
KEGG_PPAR signaling pathway	2.26	>10
KEGG_Complement and coagulation cascades	2.22	>10
KEGG_Drug metabolism cytochrome P450	2.00	2.3
KEGG_Metabolism of xenobiotics by cytochrome P450	1.98	2.3
KEGG_P53 signaling pathway	1.82	1.4
KEGG_Porphyrin and chlorophyll metabolism	1.79	1.3
KEGG_Bladder cancer	1.66	0.9
KEGG_Tyrosine metabolism[a]	1.62	0.8
KEGG_ABC transporters	1.61	0.8
KEGG_Adipocytokine signaling pathway	1.59	0.8
KEGG_Biosynthesis of unsaturated fatty acids[a]	1.58	0.8
KEGG_Drug metabolism other enzymes	1.56	0.8
KEGG_Fatty-acid metabolism[a]	1.56	0.8
KEGG_Prion diseases	1.55	0.8
KEGG_Alanine, aspartate, and glutamate metabolism[a]	1.52	0.7
KEGG_Cytokine–cytokine receptor interaction	1.51	0.7
KEGG_Valine, leucine, and isoleucine degradation[a]	1.51	0.7
KEGG_Chronic myeloid leukemia	1.48	0.7
KEGG_Cell cycle	1.47	0.7
KEGG_ErbB signaling pathway	1.44	0.6
KEGG_Starch and sucrose metabolism[a]	1.44	0.7
KEGG_Peroxisome	1.43	0.7
KEGG_Toll-like receptor signaling pathway	1.43	0.7
KEGG_Primary immunodeficiency	1.42	0.7
KEGG_Glutathione metabolism[a]	1.40	0.6
KEGG_O-glycan biosynthesis	−1.66	0.7
KEGG_Selenoamino acid metabolism[a]	−1.74	0.7

ABC, adenosine triphosphate binding cassette; DKD, diabetic kidney disease; FDR, false discovery rate; GSEA, gene set enrichment analysis; KEGG, Kyoto Encyclopdia of Genes and Genomes; NES, normalized enrichment score; PPAR, peroxisome proliferator activated receptor.
Gene sets with FDR < 0.25 are raised in the table. The gene sets with NES > 0 were upregulated and those with NES < 0 were downregulated in group B (DKD) compared with group A (sham).
[a]Gene sets related to energy metabolism.

Table 2 | Results of GSEA in group C (DKD = enarodustat)/B (DKD)

KEGG canonical pathway (FDR < 0.25)		
Gene sets	NES	−Log$_{10}$ (FDR)
KEGG_Pentose phosphate pathway[a]	2.22	>10
KEGG_RIG-I–like receptor signaling pathway	1.88	1.4
KEGG_Glycolysis, gluconeogenesis[a]	1.88	1.6
KEGG_Fructose and mannose metabolism[a]	1.79	1.3
KEGG_Primary immunodeficiency	1.76	1.3
KEGG_DNA replication	1.73	1.3
KEGG_Systemic lupus erythematosus	1.70	1.2
KEGG_Complement and coagulation cascades	1.66	1.1
KEGG_Cytosolic DNA-sensing pathway	1.64	1.1
KEGG_Prion diseases	1.60	1.0
KEGG_P53-signaling pathway	1.58	1.0
KEGG_Galactose metabolism[a]	1.58	1.0
KEGG_Cytokine–cytokine receptor interaction	1.54	1.0
KEGG_Hematopoietic cell lineage	1.54	1.0
KEGG_Toll-like receptor signaling pathway	1.52	1.0
KEGG_Cell cycle	1.49	0.9
KEGG_Cell adhesion molecules (CAMs)	1.41	0.7
KEGG_Progesterone-mediated oocyte maturation	1.36	0.6
KEGG_Proximal tubule bicarbonate reclamation	−1.47	0.8
KEGG_Retinol metabolism	−1.47	0.8
KEGG_Butanoate metabolism	−1.49	0.8
KEGG_Spliceosome	−1.49	0.8
KEGG_Histidine metabolism[a]	−1.49	0.8
KEGG_Fatty-acid metabolism[a]	−1.50	0.8
KEGG_Tyrosine metabolism[a]	−1.58	1.1
KEGG_One carbon pool by folate[a]	−1.59	1.1
KEGG_Alanine, aspartate, and glutamate metabolism[a]	−1.61	1.1
KEGG_Peroxisome	−1.64	1.2
KEGG_RNA polymerase	−1.64	1.2
KEGG_Propanoate metabolism	−1.66	1.2
KEGG_Oxidative phosphorylation[a]	−1.66	1.2
KEGG_Steroid hormone biosynthesis	−1.71	1.4
KEGG_Metabolism of xenobiotics by cytochrome P450	−1.75	1.6
KEGG_Pyruvate metabolism[a]	−1.78	1.7
KEGG_Glycine, serine, and threonine metabolism[a]	−1.80	1.8
KEGG_Valine, leucine, and isoleucine degradation[a]	−1.82	1.8
KEGG_Citrate cycle (TCA cycle)[a]	−1.89	2.2
KEGG_Aminoacyl-tRNA biosynthesis	−1.92	2.4
KEGG_Drug metabolism cytochrome P450	−1.93	2.2
KEGG_Tryptophan metabolism[a]	−2.15	2.9

DKD, diabetic kidney disease; FDR, false discovery rate; GSEA, gene set enrichment analysis; KEGG, Kyoto Encyclopdia of Genes and Genomes; NES, normalized enrichment score; RIG-I, retinoic acid inducible gene I; TCA, tricarboxylic acid; tRNA, transfer RNA.
Gene sets with FDR < 0.25 are raised in the table. The gene sets with NES > 0 were upregulated and those with NES < 0 were downregulated in group C (DKD + enarodustat) compared with group B (DKD).
[a]Gene sets related to energy metabolism.

transcriptome and metabolome data has demonstrated that enarodustat counteracts renal energy metabolism alterations occurring in the early stages of DKD.

Symmetric metabolism alterations (diabetes vs. enarodustat) are confirmed in an alternative model

We conducted transcriptome analysis in alloxan-induced diabetic mice, another animal model of diabetes, to confirm our findings in the rat model. Study protocols and background data for the mouse model are shown in Figure 9. Urinary albumin excretion was significantly increased in group B compared with group A, which was reversed by enarodustat (Figure 9d). In addition, we applied comprehensive 3-dimensional analysis (Clear, Unobstructed Brain/Body Imaging Cocktails, and Computational analysis [CUBIC]–kidney)[16] to visualize glomeruli in the kidney. Glomerulomegaly was noticeable in group B compared with group A, which was reversed by enarodustat (Figure 9e). Transcriptome analysis of renal tissue in alloxan-induced diabetic mice showed symmetric metabolism alterations (diabetes vs. enarodustat) in the same way as in the STZ-induced diabetic rat model (Figure 10): fatty-acid metabolism was upregulated by diabetes, whereas glucose metabolism was upregulated by enarodustat. Furthermore, amino-acid metabolism was upregulated by diabetes and downregulated by enarodustat. Thus, enarodustat counteracted renal energy metabolism alterations occurring in the early stages of DKD in the alloxan-induced diabetic mouse model as well as in the STZ-induced diabetic rat model.

a Group B (DKD)/A (Sham)

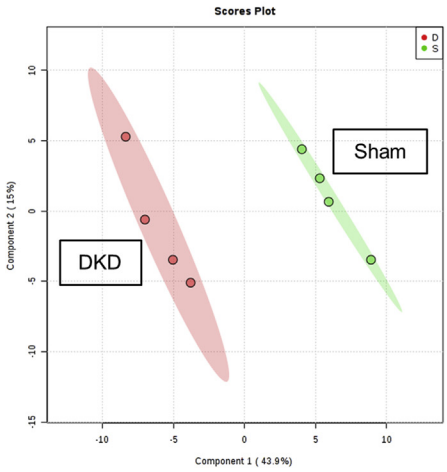

MetaboAnalyst MSEA (FDR < 0.05)

Metabolite sets	Total	Hits	$-\log_{10}$ (*P* value)	$-\log_{10}$ (FDR)
Glycine and serine metabolism	59	11	4.1	2.2
Methionine metabolism	43	9	3.8	2.2
Warburg effect	58	10	3.5	2.1
Urea cycle	29	7	3.5	2.1
Purine metabolism	74	11	3.2	1.9
Aspartate metabolism	35	7	2.9	1.7
Glutamate metabolism	49	8	2.7	1.6
Pentose phosphate pathway	29	6	2.7	1.6
Arginine and proline metabolism	53	8	2.5	1.4
Ammonia recycling	32	6	2.4	1.4
Beta-alanine metabolism	34	6	2.3	1.3

Metabolites with PLS-DA VIP ≥ 1 (51 metabolites)
Amino acid metabolism

b Group C (DKD + enarodustat)/B (DKD)

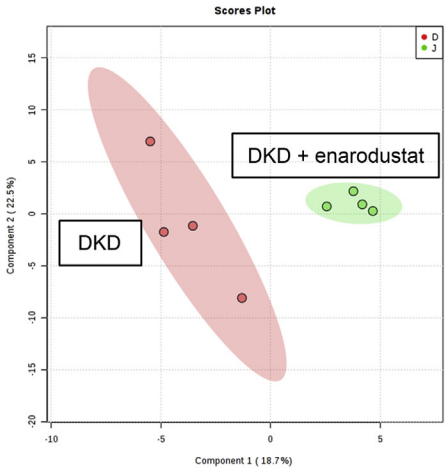

MetaboAnalyst MSEA (FDR < 0.05)

Metabolite sets	Total	Hits	$-\log_{10}$ (*P* value)	$-\log_{10}$ (FDR)
Warburg effect	58	9	3.4	1.7
Glycine and serine metabolism	59	9	3.3	1.7
Arginine and proline metabolism	53	8	3.0	1.5
Ammonia recycling	32	6	2.8	1.4
Aspartate metabolism	35	6	2.6	1.4
Gluconeogenesis	35	6	2.6	1.4
Glycolysis	25	5	2.5	1.4
Glutamate metabolism	49	7	2.5	1.4

Metabolites with PLS-DA VIP ≥ 1 (43 metabolites)
Glycolysis, gluconeogenesis
Amino acid metabolism

Figure 7 | Partial least squares discriminant analysis (PLS-DA) and metabolite set enrichment analysis (MSEA) using the metabolome data. The absolute concentrations of 116 energy-related-metabolites were measured in renal cortical tissue of rats ($n = 4$, for each group) randomly selected from each group (see Supplementary Figure S3). (**a**) PLS-DA scores plot of group B (diabetic kidney disease [DKD])/A (sham) is shown on the left side. MSEA was conducted using metabolites with the PLS-DA variable importance in projection (VIP) score ≥ 1 (51 metabolites, Supplementary Table S2). The MSEA results (shown on the right side) suggest changes in amino-acid metabolism (highlighted in green). (**b**) PLS-DA scores plot of group C (DKD + enarodustat)/B is shown on the left side. MSEA was conducted using metabolites with the PLS-DA VIP score ≥ 1 (43 metabolites, Supplementary Table S3). The MSEA results (shown on the right side) suggest changes in glycolysis and gluconeogenesis (highlighted in brown) and in amino-acid metabolism (highlighted in green). FDR, false discovery rate.

DISCUSSION

In this study, we have demonstrated that enarodustat (JTZ-951), an oral HIF stabilizer, counteracts renal energy metabolism alterations occurring in the early stages of DKD in rat and mouse models of diabetes. Transcriptome and metabolome analyses have shown symmetric metabolism alterations in renal tissue (diabetes vs. enarodustat): fatty-acid and amino-acid metabolisms were upregulated in DKD, whereas enarodustat downregulated these pathways and additionally upregulated glucose metabolism (Figures 5–10).

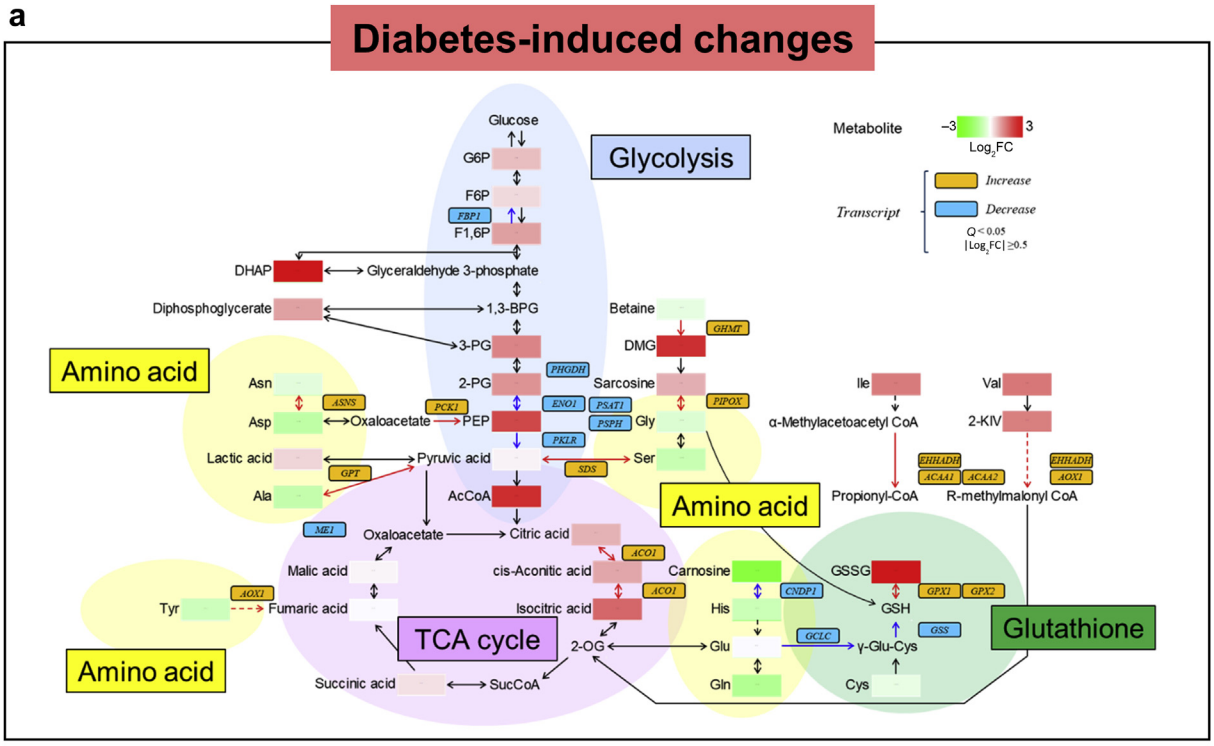

Metabolic reprogramming by HIF stabilization counteracts renal metabolism alterations in the early stages of diabetic kidney disease.

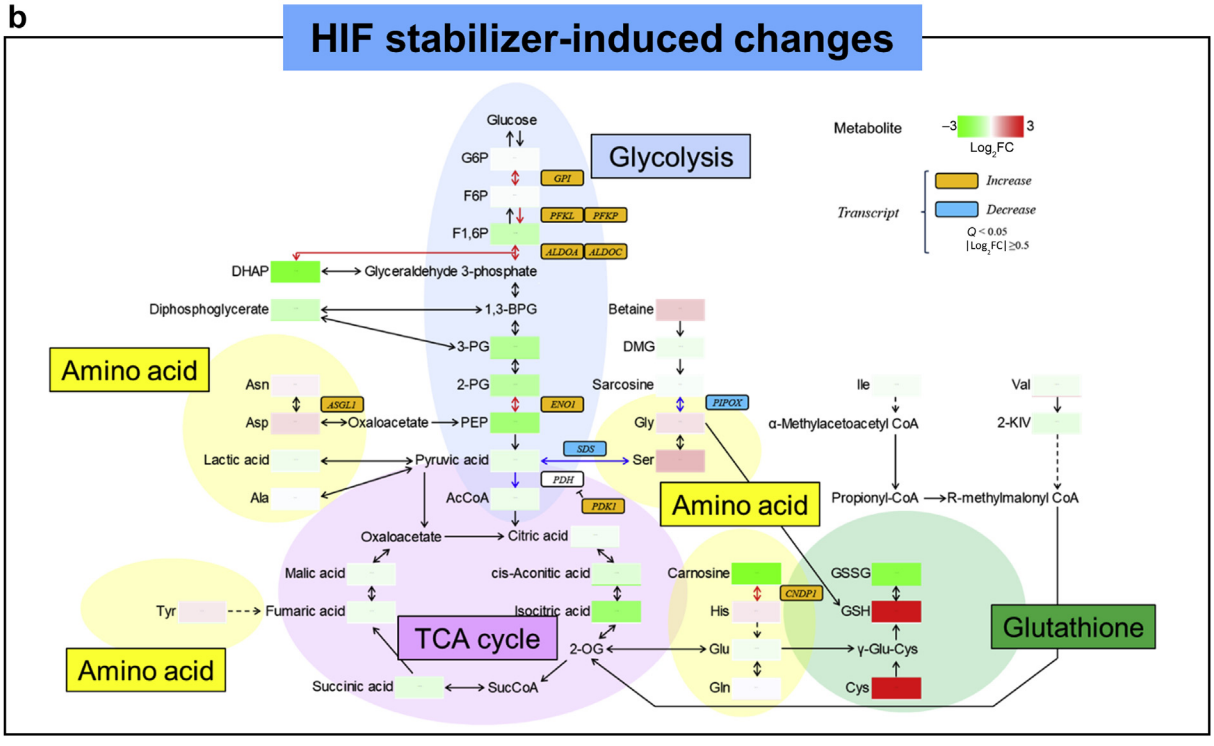

It has not been fully elucidated whether HIF stabilization has protective effects on the pathophysiology of DKD or not. Previous studies have shown that diabetic renal tissue is exposed to hypoxia[17] and HIF expression in diabetic renal tissue is insufficient in responding to their hypoxic conditions, which is partially caused by oxidative stress.[18] HIF stabilization by cobalt chloride improved oxidative stress status and reduced proteinuria and tubulointerstitial damage in STZ-induced DKD.[19] Animal study results also indicated that HIF stabilization protected against the development of obesity,[20] improved insulin sensitivity,[20] and lowered serum cholesterol levels.[21] These results suggest the protective effects of HIF stabilization in the development of DKD. In contrast, supraphysiologic HIF stabilization by von Hippel-Lindau deletion was reported to induce renal fibrosis.[22] The role of HIF stabilization in DKD progression may be context-dependent given the pleiotropic effects of HIF and the existence of varied DKD phenotypes.

The aim of this study was to clarify the net effects of HIF stabilization on energy metabolism in diabetic kidney. Previous reports have indicated that energy metabolism alterations occur in DKD. Sas *et al.*[10] showed increased energy metabolic flux and accumulation of glucose metabolites in diabetic renal cortical tissue, which might be related to mitochondrial dysfunction. You *et al.*[23] reported that fumarate, a TCA cycle metabolite, was accumulated in diabetic renal tissue and it directly contributed to the progression of DKD. We have previously shown that TCA cycle metabolites accumulated in diabetic renal tissue, which was reversed by sodium–glucose cotransporter 2 inhibition or calorie restriction.[11] Moreover, Qi *et al.*[24] showed that enzymes in glycolytic pathways including pyruvate kinase M2 (PKM2), were upregulated in type 1 diabetic patients without DKD compared with patients with DKD. PKM2 activation reversed the accumulation of glycolysis metabolites and restored mitochondrial function, partially by increasing glycolytic flux.[24,25] These previous reports suggest that accumulation of glycolysis and TCA cycle metabolites might affect the progression of DKD, which can be mitigated by facilitated glycolysis including PKM2 activation.

In our study, HIF stabilization by enarodustat reversed energy metabolism alterations and mitigated the accumulation of glycolysis and TCA cycle metabolites in diabetic renal cortical tissue (Figure 8). The expression of glycolytic enzymes including PKM2 was also upregulated by enarodustat (Supplementary Figure S4B). Moreover, enarodustat alleviated GSSG accumulation and increased the glutathione/GSSG ratio, which suggests that enarodustat relieved the oxidative stress in DKD (Figure 8). This enarodustat-induced reduction in oxidative stress was also confirmed by changes in malondialdehyde levels in renal cortical tissue (Supplementary Figure S4A). These results suggest that HIF stabilization should have protective roles on the pathophysiology of DKD at least from metabolic perspectives.

It is certain that we cannot examine whether the metabolic reprogramming by HIF stabilization has direct effects on DKD progression, because it may be impossible to discern the net effects of metabolism alterations on the renal outcome due to the pleiotropic role of HIF. However, in our study, mild urinary albumin excretion and renal pathological abnormalities (glomerulomegaly and glomerular basement membrane thickening) induced by diabetes were mitigated by enarodustat, in association with the normalization of renal energy metabolism. We extracted the genes whose expression changes correlated with urinary albumin levels (257 probes; 232 genes) from the microarray data in alloxan-induced diabetic mouse model and conducted pathway enrichment analysis (Supplementary Figure S5). As a result, pathways related to mitochondrial membrane and respiratory electron transport are upregulated associated with urinary albumin levels, indicating that mitochondrial burden is closely related to urinary albumin excretion. Thus, there is a possibility that the metabolic normalization of diabetic renal tissue by HIF stabilizers might reduce the mitochondrial burden and mitigate the progression of DKD. Our data suggest the pathophysiology of DKD from metabolic perspectives as follows: Hyperglycemia creates energy demand for glucose reabsorption in renal proximal tubules; thus, TCA cycle in mitochondria is forcibly activated to meet the energy demand in the early stages of DKD (upregulation of fatty-acid and

Figure 8 | Visualization of transcriptome and metabolome data on the energy metabolic pathway map. (**a**) Transcriptome and metabolome data of group B (diabetic kidney disease [DKD])/A (sham) are visualized (diabetes-induced changes). Accumulation of glycolysis and tricarboxylic acid (TCA) cycle metabolites, amino-acid consumption, and glutathione disulfide (GSSG) accumulation can be recognized in group B (DKD) compared with group A (sham). (**b**) Transcriptome and metabolome data of group C (DKD + enarodustat)/B are visualized (hypoxia-inducible factor [HIF] stabilizer-induced changes). Metabolic reprogramming by enarodustat counteracted the diabetes-induced metabolism alterations in renal tissue. *ACAA1* (*2*), acetyl-CoA acyltransferase 1 (2); AcCoA, acetyl coenzyme A; *ACO1*, aconitase 1; Ala, alanine; *ALDOA (C)*, aldolase, fructose-bisphosphate A (C); *AOX1*, aldehyde oxidase 1; *ASGL1*, L-asparaginase; Asn, asparagine; *ASNS*, asparagine synthetase; Asp, aspartate; BPG, bisphosphoglycerate; *CNDP1*, carnosine dipeptidase 1; CoA, coenzyme A; Cys, cysteine; DHAP, dihydroxyacetone phosphate; DMG, dimethylglycine; *EHHADH*, enoyl-CoA hydratase and 3-hydroxyacyl CoA dehydrogenase; *ENO1*, enolase 1; *FBP1*, fructose-1,6-biphosphatase 1; FC, fold-change; *GCLC*, glutamate-cysteine ligase catalytic subunit; Gln, glutamine; Glu, glutamate; Gly, glycine; *GNMT*, glycine N-methyltransferase; *GPI*, glucose-6-phosphate isomerase; *GPT*, glutamic–pyruvic transaminase; *GPX1* (*2*), glutathione peroxidase 1 (2); GSH, glutathione; *GSS*, glutathione synthetase; His, histidine; KIV, alpha-ketoisovaleric acid; *ME1*, malic enzyme 1; OG, oxoglutarate; *PCK1*, phosphoenolpyruvate carboxykinase 1; *PDK1*, pyruvate dehydrogenase kinase 1; *PDH*, pyruvate dehydrogenase; PEP, phosphoenolpyruvate; *PFKL*, phosphofructokinase, liver type; *PFKP*, phosphofructokinase, platelet; PG, prostaglandin; *PHGDH*, phosphoglycerate dehydrogenase; *PIPOX*, pipecolic acid and sarcosine oxidase; *PKLR*, pyruvate kinase L/R; *PSAT1*, phosphoserine aminotransferase 1; *PSPH*, phosphoserine phosphatase; *SDS*, serine dehydratase; Ser, serine; SucCoA, succinyl coenzyme A; Tyr, tyrosine; Val, valine.

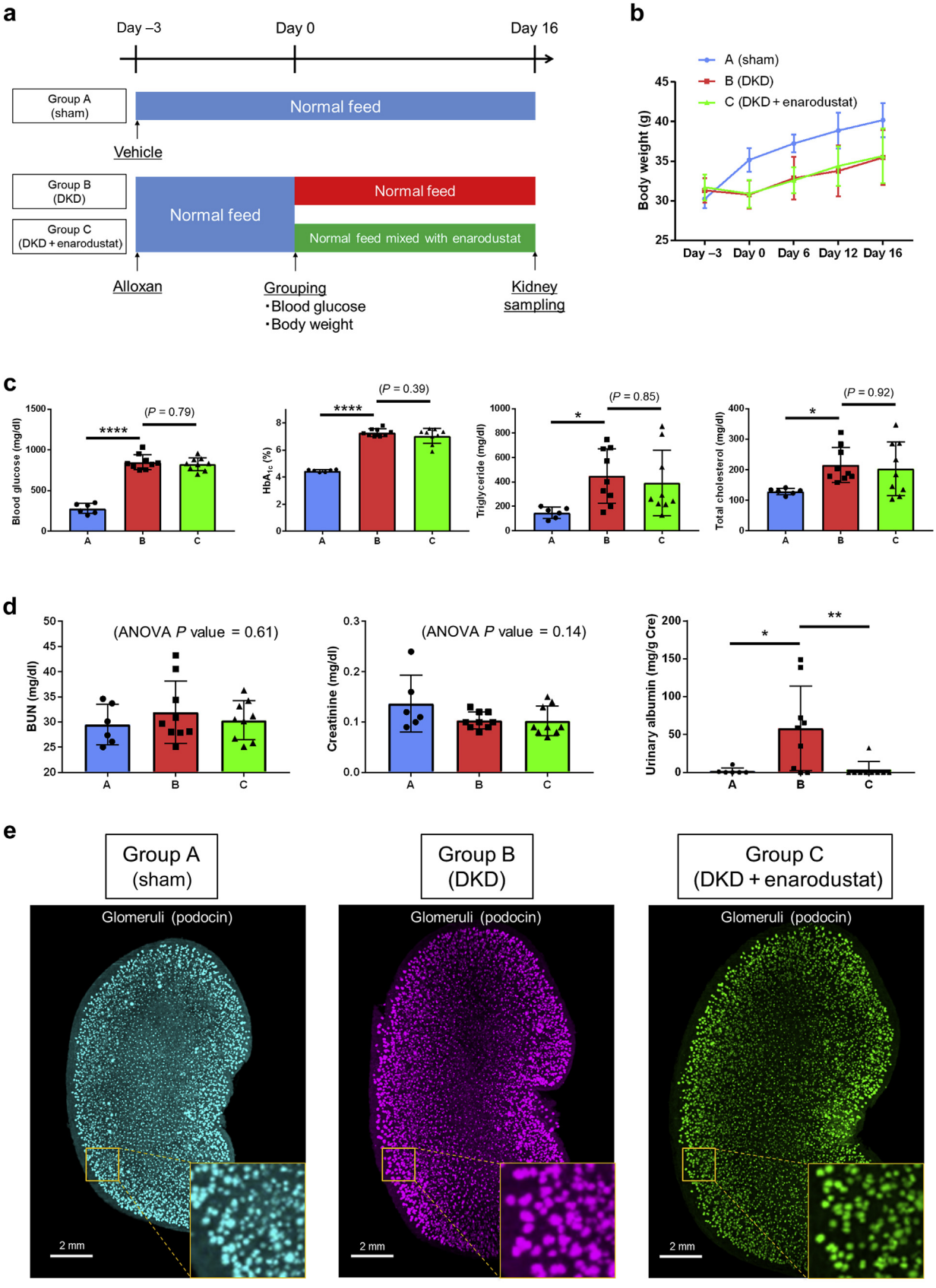
a
Day –3
Day 0
Day 16
Group A (sham)
Normal feed
Vehicle
Group B (DKD)
Group C (DKD + enarodustat)
Normal feed
Normal feed
Normal feed mixed with enarodustat
Alloxan
Grouping
・Blood glucose
・Body weight
Kidney sampling
b
A (sham)
B (DKD)
C (DKD + enarodustat)
Body weight (g)
Day –3
Day 0
Day 6
Day 12
Day 16
c
Blood glucose (mg/dl)
(P = 0.79)
HbA1c (%)
(P = 0.39)
Triglyceride (mg/dl)
(P = 0.85)
Total cholesterol (mg/dl)
(P = 0.92)
d
BUN (mg/dl)
(ANOVA P value = 0.61)
Creatinine (mg/dl)
(ANOVA P value = 0.14)
Urinary albumin (mg/g Cre)
e
Group A (sham)
Group B (DKD)
Group C (DKD + enarodustat)
Glomeruli (podocin)
2 mm

amino-acid metabolism). And HIF stabilizers might mitigate this mitochondrial burden by the metabolic reprogramming from TCA cycle to glycolysis (downregulation of fatty-acid and amino-acid metabolism and upregulation of glycolysis), which might have protective roles against DKD progression. Further studies including single-cell omics are needed to clarify how the mitochondrial burden in renal tissue directly affects the pathophysiology of DKD.

Another interesting question is whether HIF stabilizers directly affect the glucose absorption in proximal tubules. Our *in vitro* data showed that ATP production is significantly reduced by enarodustat through metabolic reprogramming from TCA cycle to glycolysis (Figures 1 and 2). Considering that ATP is required for glucose reabsorption by sodium–glucose cotransporter 2, we first hypothesized that glucose reabsorption might be inactivated by enarodustat. However, urinary glucose levels were not significantly different between group B and group C in both animal models (Supplementary Figure S6). Probably, the reduction in ATP production by enarodustat is much milder in a physiological situation compared with its effect *in vitro*; thus, HIF stabilization does not affect glucose absorption through sodium–glucose cotransporter 2, at least in our animal experiments.

Our study had 2 limitations. First, we utilized STZ-induced diabetic rats and alloxan-induced diabetic mice as early-stage DKD models and observed the short-term effects of diabetic conditions. However, in the clinical setting, HIF stabilizers would be administered to patients with anemia in late-stage DKD. More studies are needed to understand the effect of HIF stabilization on renal metabolism alterations in late-stage DKD. Second, the study lacked sufficient statistical power with respect to the dispersion of metabolites' concentrations in the metabolome data, whereas the transcriptome data had statistical power large enough to clarify the whole picture of energy metabolism. Because not many metabolites showed significant difference between groups, we conducted PLS-DA and selected the metabolites with PLS-DA VIP score ≥ 1 for MSEA. Although it is difficult to cross-verify a metabolic change using metabolomics data alone, the results of metabolome analysis were compatible with the transcriptomic data (Figures 7 and 8), providing additional support for the observed effects of transcriptome alterations on renal energy metabolism.

In conclusion, enarodustat (JTZ-951), an oral HIF stabilizer, counteracts renal energy metabolism alterations in the early stages of DKD. Our study suggests that HIF stabilization may serve as a potential intervention that targets the dysregulated renal energy metabolism in DKD.

METHODS

Mito Stress Test and Glycolytic Rate Assay

HK-2 cells[15] were seeded onto a 96-well microplate at a density of 1×10^4 cells/well. On the next day, metabolic flux was measured in real time by Seahorse XFe96 Analyzer (Agilent) using Mito Stress Test Kit (103015-100; Agilent) or Glycolytic Rate Assay Kit (103344-100; Agilent). Concentrations of glucose, pyruvate, and glutamine in culture media were 10 mmol/l, 1 mmol/l, and 2 mmol/l, respectively.

siRNA transfection

HIF-1 knockdown was conducted by Stealth RNAi for human HIF1A (HSS104774 [#1] and HSS104775 [#2]; Thermo Fisher Scientific, Waltham, MA). Stealth RNAi siRNA Negative Control Med GC Duplex #2 (12935112; Thermo Fisher Scientific) was used as the negative control.

Western blotting

Primary antibodies used for staining were anti-human HIF-1α antibody (rabbit polyclonal, 1:500; Novus Biologicals, Littleton, CO) and anti-human actin antibody (rabbit polyclonal, 1:1000; Sigma-Aldrich, St. Louis, MO). Secondary antibody was the horseradish peroxidase-conjugated goat anti-rabbit IgG antibody (170-6515, 1:5000; Bio-Rad Laboratories, Hercules, CA).

Animal experiments

Crl:CD (Sprague Dawley) rats and Crl:CD1 (Institute of Cancer Research) mice were obtained from Charles River Laboratories Japan Inc. (Yokohama, Japan). All experiments were approved by the University of Tokyo Institutional Review Board (approval number P17-110). All animal procedures were performed according to the National Institutes of Health guidelines (*Guide for the Care and Use of the Laboratory Animals*). Study protocols are shown in Figures 3 and 9.

Transcriptome analysis

Total RNA from renal cortical tissue was isolated using GenElute Mammalian Total RNA Miniprep Kit (RTN70; Sigma-Aldrich). Total RNA (100 ng) was labeled using Low Input Quick Amp Labeling Kit (Agilent) and then hybridized to SurePrint G3 Rat GE v2 8x60K Microarray (for rat; Agilent) and SurePrint G3 Mouse GE v2 8x60K Microarray (for mouse), respectively. All microarray experiments were performed by DNA Chip Research Inc. (Tokyo, Japan). Raw data were processed with the R package limma in Bioconductor (http://www.bioconductor.org/) to perform background correction and data normalization using the quantile normalization method. Batch effects were removed by ComBat[26,27] (Bioconductor) in the rat

Figure 9| Study protocols, background data, and 3-dimensional pathologies of alloxan-induced diabetic mice. (**a**) Study protocols of experiments in alloxan-induced diabetic mice are shown. (**b**) Transition of the body weights are shown. Body weights were not significantly different between group B (diabetic kidney disease [DKD]) and group C (DKD + enarodustat). (**c**) Blood glucose, glycosylated hemoglobin HbA_{1c}, triglyceride, and total cholesterol levels on day 16 are shown. (**d**) Blood urea nitrogen (BUN), plasma creatinine (Cre), and urinary albumin levels on day 16 are shown. Urinary albumin excretion was significantly increased in group B compared with group A (sham), which was reversed by enarodustat. (**e**) Comprehensive 3-dimensional imaging (Clear, Unobstructed Brain/Body Imaging Cocktails, and Computational analysis [CUBIC]–kidney) of glomeruli is shown. Glomerulomegaly was noticeable in group B compared with group A, which was reversed by enarodustat. All data are expressed as mean ± SD. For multiplex comparisons, 1-way analysis of variance (ANOVA) was applied, followed by the Tukey multiple comparisons test, if appropriate (*$P < 0.05$, **$P < 0.01$, ****$P < 0.0001$). To optimize viewing of this image, please see the online version of this article at www.kidney-international.org.

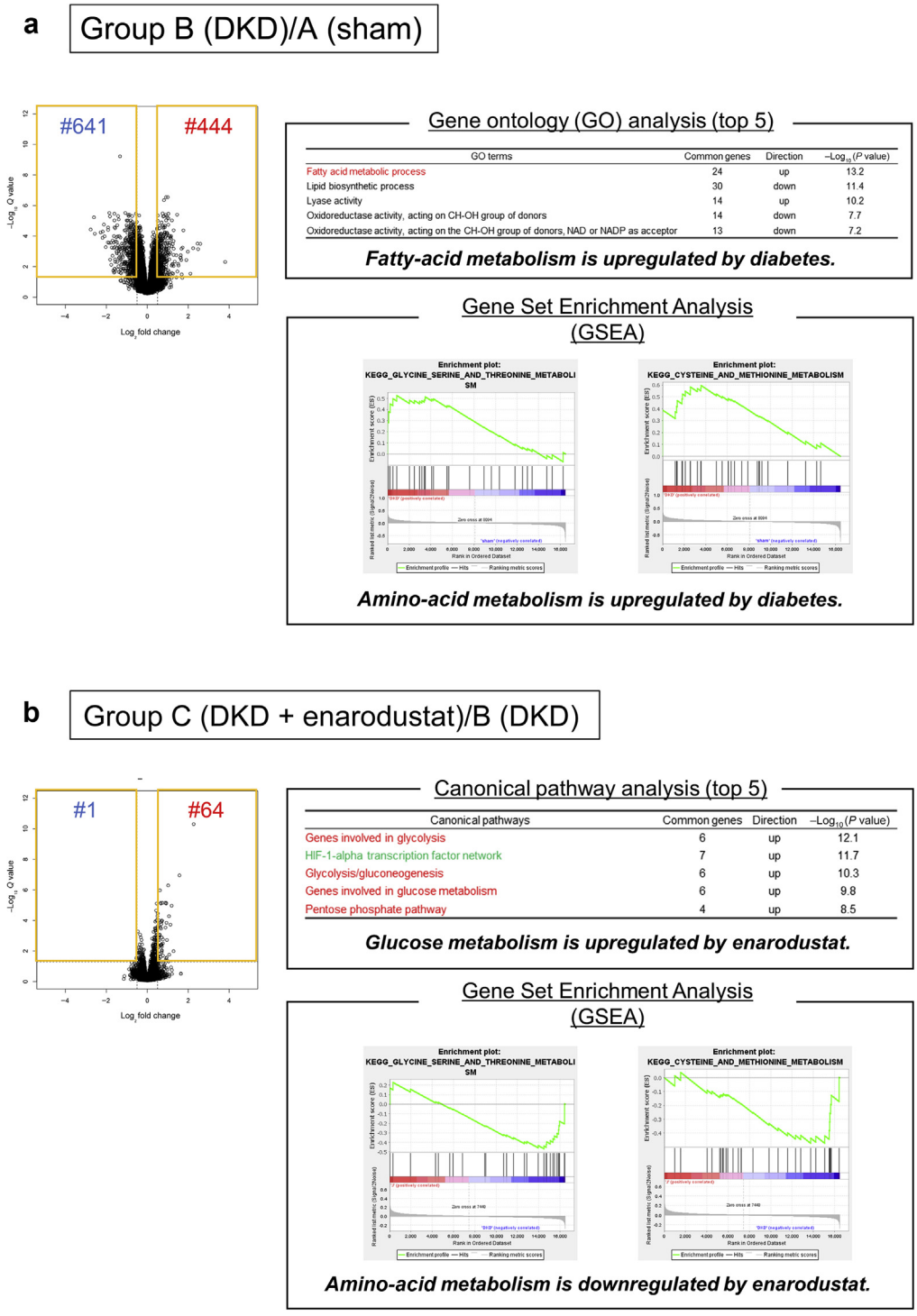

Figure 10 | Transcriptome analysis of renal tissue in alloxan-induced diabetic mice. Symmetric metabolism alterations (diabetes vs. enarodustat) were confirmed by transcriptome analysis of renal tissue in alloxan-induced diabetic mice. (**a**) Gene ontology (GO) analysis of differentially expressed genes (DEGs) and gene set enrichment analysis (GSEA) in group B (diabetic kidney disease [DKD])/A (sham). DEGs were selected by $|\log_2$ fold-change (FC)$| \geq 0.5$ and Q value < 0.05 (1085 probes). Fatty-acid and amino-acid metabolisms were upregulated by diabetes. (**b**) Canonical pathway analysis of DEGs and GSEA in group C (DKD + enarodustat)/B. DEGs were selected as described (65 probes). Glucose metabolism was upregulated, and amino-acid metabolism was downregulated by enarodustat. HIF-1, hypoxia-inducible factor 1; NAD, nicotinamide adenine dinucleotide; NADP, NAD phosphate.

experiment. Differentially expressed genes were determined by $|\log_2$ FC$| \geq 0.5$ and Q value < 0.05. Gene ontology and canonical pathway analyses were conducted using BaseSpace Correlation Engine (Illumina, San Diego, CA). Microarray data have been deposited in the National Center for Biotechnology Information Gene Expression Omnibus as series GSE131221 (rat) and GSE139317 (mouse).

Gene Set Enrichment Analysis

GSEA is a computational method that determines whether an *a priori*–defined set of genes shows statistically significant, concordant differences between 2 biological states.[28,29] GSEA was performed using GSEA v.3.0 (Broad Institute, Cambridge, MA). The pathways with a false discovery rate < 0.25 were considered significant.

Metabolome analysis

Metabolome measurements were performed by Human Metabolome Technologies Inc. (Tsuruoka, Japan).[30,31] Metabolite concentrations were calculated by normalizing the peak area of each metabolite with respect to the area of the internal standard and by using standard curves, which were obtained from 3-point calibrations. See also the Supplementary Methods.

Metabolite set enrichment analysis

The analysis of metabolomics data was conducted using the integrated web-based platform MetaboAnalyst 4.0.[32] PLS-DA was performed and associated VIP scores were calculated. The metabolites with PLS-DA VIP score ≥ 1 were used for the MSEA.

Quantification of glomerular areas in renal pathologies

We randomly took 3 pathological pictures from each sample's periodic acid–Schiff staining image and measured every glomerular area respectively using Fiji (a distribution of ImageJ; National Institutes of Health, Bethesda, MD).[33]

CUBIC-kidney

Comprehensive 3-dimensional imaging of glomeruli in renal tissue was performed using CUBIC according to our previous papers.[16,34–36] In brief, fixed mouse kidneys were immersed in CUBIC-L for delipidation and then subjected to immunofluorescent staining. Finally, the refractive index was matched by the placement of the samples in CUBIC-R+.[16] Comprehensive 3D–dimensional images from transparent kidneys were acquired with a custom-built light-sheet fluorescence microscopy (MVX10-LS; Olympus, Tokyo, Japan).[37,38] Primary antibody used for staining was anti-podocin antibody (rabbit polyclonal, 1:100, P0372; Sigma-Aldrich). Secondary antibody was Alexa Flour 555-conjugated donkey anti-rabbit IgG (1:100, A-31572; Invitrogen, Thermo Fisher Scientific).

Statistical analysis

For multiplex comparisons, 1-way analysis of variance followed by the *post hoc* Tukey multiple comparisons test, if appropriate, was applied. All statistical analyses were performed with GraphPad Prism 7 software (GraphPad Software, San Diego, CA). $P < 0.05$ was considered statistically significant. Data are presented as the mean ± SD.

DISCLOSURE

MN has received honoraria, advisory fees, or research funding from Kyowa-Hakko-Kirin, Akebia, Astellas, Chugai, GlaxoSmithKline, Japan Tobacco Inc. (JT), Torii, Tanabe-Mitsubishi, Daiichi-Sankyo, Takeda, Ono, Bayer, Boehringer Ingelheim and Alexion. TT has received a research grant from JT. Enarodustat (JTZ-951) was provided by JT, Tokyo, Japan. EAS and HRU are coinventors of patents owned by RIKEN. Part of this study was done in collaboration with Olympus Corporation and kind software supports by Bitplane. The other author declared no competing interests.

ACKNOWLEDGMENTS

We are grateful to Dr. Shuhei Yao and Dr. Shinji Tanaka for valuable discussions. We also thank Dr. Tsuyoshi Inoue, Dr. Satoru Fukuda, and Ms. Kahoru Amitani for their technical support. This work was partially carried out under the support of Isotope Science Center, the University of Tokyo. This work was supported by Grant-in-Aid for Japan Society for the Promotion of Science (JSPS) Research Fellow (JSPS KAKENHI grant 19J11928 to SH), Grant-in-Aid for Scientific Research (B) (JSPS KAKENHI grant 18H02824 to MN), Grant-in-Aid for Scientific Research (C) (JSPS KAKENHI grant 17K09688 to TT), and Grant-in-Aid for Scientific Research on Innovative Areas (KAKENHI grant 26111003 to MN).

SUPPLEMENTARY MATERIAL

Supplementary Methods.

Figure S1. Additional parameters of Mito Stress Test and Glycolytic Rate Assay. (**A**) The results of maximal respiration, spare respiratory capacity and ATP production measured by Mito Stress Test are shown ($n = 36$ for each group, $^{****}P < 0.0001$). (**B**) Compensatory glycolysis measured by Glycolytic Rate Assay is shown ($n = 36$ for each group, $^{****}P < 0.0001$). All data are expressed as mean ± SD.

Figure S2. Mito Stress Test with another siRNA (#2) for hypoxia-inducible factor-1 (HIF-1). (**A**) The experiments using another siHIF-1 (#2) showed the same results as with siHIF-1 (#1) illustrated in Figure 2. O_2 consumption rates (OCR) were measured in real time under basal conditions and in response to indicated mitochondrial inhibitors (oligomycin, FCCP, and Rot/AA). (**B**) HIF-1 knockdown reversed decreases in OCR parameters (basal respiration, maximal respiration, spare respiratory capacity and ATP production) induced by enarodustat ($n = 18$ for each group, $^{****}P < 0.0001$). All data are expressed as mean ± SD.

Figure S3. The absolute concentration of 116 metabolites related to energy metabolism in renal cortical tissue. The absolute concentrations of 116 energy-related-metabolites in renal cortical tissue of rats' experiments were shown. All data are expressed as mean ± SD.

Figure S4. Additional data from streptozotocin-induced diabetic rats. (**A**) Malondialdehyde (MDA) levels in renal cortical tissue are shown; MDA is a lipid peroxidation marker that indicates the degree of oxidative stress. MDA level was increased in diabetic renal cortical tissue and enarodustat reversed it. (**B**) Quantitative polymerase chain reaction (qPCR) data of pyruvate kinase muscle isozyme M2 (PKM2) are shown; enarodustat significantly increased the level of PKM2 mRNA in diabetic renal tissue. For multiplex comparisons, 1-way analysis of variance (ANOVA) was applied, followed by the Tukey multiple comparisons test, if appropriate ($^{*}P < 0.05$, $^{**}P < 0.01$, $^{***}P < 0.001$). All data are expressed as mean ± SD.

Figure S5. Pathway enrichment analysis using genes correlated with urinary albumin levels in alloxan-induced mouse model. We extracted the genes whose expression levels correlated with urinary albumin levels (Pearson correlation coefficient: $|r| > 0.5$) from the microarray data in alloxan induced diabetic mouse model (257 probes; 232 genes). The results of pathway enrichment analysis using the extracted genes are shown. Genes related to the mitochondrial membrane and respiratory electron transport (highlighted in red) were upregulated.

Figure S6. Urinary glucose levels in rat and mouse animal models of diabetes. (**A**) Urinary glucose levels of streptozotocin (STZ)-induced diabetic rats are shown. (**B**) Urinary glucose levels of alloxan-induced diabetic mice are shown. Enarodustat did not alter urinary glucose levels. For multiplex comparisons, 1-way analysis of variance (ANOVA) was applied, followed by the Tukey multiple comparisons test, if appropriate ($^{****}P < 0.0001$). All data are expressed as mean ± SD.

Table S1. The absolute concentrations of 116 energy-related-metabolites in renal cortical tissue. The absolute concentrations of 116 energy-related-metabolites in renal cortical tissue of rats' experiments are shown. N.D., not detected.

Table S2. Metabolites for metabolite set enrichment analysis (MSEA) between group A (sham) and B (DKD). Metabolites were selected by partial least squares discriminant analysis (PLS-DA) variable importance in projection (VIP) score ≥ 1.
Table S3. Metabolites for metabolite set enrichment analysis (MSEA) between group B (DKD) and C (DKD + enarodustat). Metabolites were selected by partial least squares discriminant analysis (PLS-DA) variable importance in projection (VIP) score ≥ 1.
Supplementary material is linked to the online version of the paper at www.kidney-international.org.

REFERENCES

1. Hasegawa S, Tanaka T, Nangaku M. Hypoxia-inducible factor stabilizers for treating anemia of chronic kidney disease. *Curr Opin Nephrol Hypertens*. 2018;27:331–338.
2. Maxwell P. HIF-1: an oxygen response system with special relevance to the kidney. *J Am Soc Nephrol*. 2003;14:2712–2722.
3. Marx J. Cell biology: how cells endure low oxygen. *Science*. 2004;303:1454–1456.
4. Nangaku M. Chronic hypoxia and tubulointerstitial injury: a final common pathway to end-stage renal failure. *J Am Soc Nephrol*. 2006;17:17–25.
5. Tanaka T, Miyata T, Inagi R, et al. Hypoxia in renal disease with proteinuria and/or glomerular hypertension. *Am J Pathol*. 2004;165:1979–1992.
6. Kim JW, Tchernyshyov I, Semenza GL, et al. HIF-1-mediated expression of pyruvate dehydrogenase kinase: a metabolic switch required for cellular adaptation to hypoxia. *Cell Metab*. 2006;3:177–185.
7. Papandreou I, Cairns RA, Fontana L, et al. HIF-1 mediates adaptation to hypoxia by actively downregulating mitochondrial oxygen consumption. *Cell Metab*. 2006;3:187–197.
8. Thomas MC, Cooper ME, Zimmet P. Changing epidemiology of type 2 diabetes mellitus and associated chronic kidney disease. *Nat Rev Nephrol*. 2016;12:73–81.
9. Hasegawa S, Jao TM, Inagi R. Dietary metabolites and chronic kidney disease. *Nutrients*. 2017;9:358.
10. Sas KM, Kayampilly P, Byun J, et al. Tissue-specific metabolic reprogramming drives nutrient flux in diabetic complications. *JCI Insight*. 2016;1:e86976.
11. Tanaka S, Sugiura Y, Saito H, et al. Sodium-glucose cotransporter 2 inhibition normalizes glucose metabolism and suppresses oxidative stress in the kidneys of diabetic mice. *Kidney Int*. 2018;94:912–925.
12. Sharma K. Mitochondrial dysfunction in the diabetic kidney. *Adv Exp Med Biol*. 2017;982:553–562.
13. Ogoshi Y, Matsui T, Mitani I, et al. Discovery of JTZ-951: a HIF prolyl hydroxylase inhibitor for the treatment of renal anemia. *ACS Med Chem Lett*. 2017;8:1320–1325.
14. Akizawa T, Nangaku M, Yamaguchi T, et al. A placebo-controlled, randomized trial of enarodustat in patients with chronic kidney disease followed by long-term trial. *Am J Nephrol*. 2019;49:165–174.
15. Ryan MJ, Johnson G, Kirk J, et al. HK-2: an immortalized proximal tubule epithelial cell line from normal adult human kidney. *Kidney Int*. 1994;45:48–57.
16. Hasegawa S, Susaki EA, Tanaka T, et al. Comprehensive three-dimensional analysis (CUBIC-kidney) visualizes abnormal renal sympathetic nerves after ischemia/reperfusion injury. *Kidney Int*. 2019;96:129–138.
17. Laustsen C, Lycke S, Palm F, et al. High altitude may alter oxygen availability and renal metabolism in diabetics as measured by hyperpolarized [1-(13)C]pyruvate magnetic resonance imaging. *Kidney Int*. 2014;86:67–74.
18. Rosenberger C, Khamaisi M, Abassi Z, et al. Adaptation to hypoxia in the diabetic rat kidney. *Kidney Int*. 2008;73:34–42.
19. Nordquist L, Friederich-Persson M, Fasching A, et al. Activation of hypoxia-inducible factors prevents diabetic nephropathy. *J Am Soc Nephrol*. 2015;26:328–338.
20. Rahtu-Korpela L, Karsikas S, Horkko S, et al. HIF prolyl 4-hydroxylase-2 inhibition improves glucose and lipid metabolism and protects against obesity and metabolic dysfunction. *Diabetes*. 2014;63:3324–3333.
21. Hwang S, Nguyen AD, Jo Y, et al. Hypoxia-inducible factor 1alpha activates insulin-induced gene 2 (Insig-2) transcription for degradation of 3-hydroxy-3-methylglutaryl (HMG)-CoA reductase in the liver. *J Biol Chem*. 2017;292:9382–9393.
22. Kimura K, Iwano M, Higgins DF, et al. Stable expression of HIF-1alpha in tubular epithelial cells promotes interstitial fibrosis. *Am J Physiol Renal Physiol*. 2008;295:F1023–F1029.
23. You YH, Quach T, Saito R, et al. Metabolomics reveals a key role for fumarate in mediating the effects of NADPH oxidase 4 in diabetic kidney disease. *J Am Soc Nephrol*. 2016;27:466–481.
24. Qi W, Keenan HA, Li Q, et al. Pyruvate kinase M2 activation may protect against the progression of diabetic glomerular pathology and mitochondrial dysfunction. *Nat Med*. 2017;23:753–762.
25. Zhang G, Darshi M, Sharma K. The Warburg effect in diabetic kidney disease. *Semin Nephrol*. 2018;38:111–120.
26. Johnson WE, Li C, Rabinovic A. Adjusting batch effects in microarray expression data using empirical Bayes methods. *Biostatistics*. 2007;8:118–127.
27. Leek JT, Johnson WE, Parker HS, et al. The sva package for removing batch effects and other unwanted variation in high-throughput experiments. *Bioinformatics*. 2012;28:882–883.
28. Mootha VK, Lindgren CM, Eriksson KF, et al. PGC-1alpha-responsive genes involved in oxidative phosphorylation are coordinately downregulated in human diabetes. *Nat Genet*. 2003;34:267–273.
29. Subramanian A, Tamayo P, Mootha VK, et al. Gene set enrichment analysis: a knowledge-based approach for interpreting genome-wide expression profiles. *Proc Natl Acad Sci U S A*. 2005;102:15545–15550.
30. Soga T, Heiger DN. Amino acid analysis by capillary electrophoresis electrospray ionization mass spectrometry. *Anal Chem*. 2000;72:1236–1241.
31. Sugimoto M, Wong DT, Hirayama A, et al. Capillary electrophoresis mass spectrometry-based saliva metabolomics identified oral, breast and pancreatic cancer-specific profiles. *Metabolomics*. 2010;6:78–95.
32. Chong J, Soufan O, Li C, et al. MetaboAnalyst 4.0: towards more transparent and integrative metabolomics analysis. *Nucleic Acids Res*. 2018;46:W486–W494.
33. Schindelin J, Arganda-Carreras I, Frise E, et al. Fiji: an open-source platform for biological-image analysis. *Nat Methods*. 2012;9:676–682.
34. Susaki EA, Tainaka K, Perrin D, et al. Whole-brain imaging with single-cell resolution using chemical cocktails and computational analysis. *Cell*. 2014;157:726–739.
35. Tainaka K, Kubota SI, Suyama TQ, et al. Whole-body imaging with single-cell resolution by tissue decolorization. *Cell*. 2014;159:911–924.
36. Susaki EA, Tainaka K, Perrin D, et al. Advanced CUBIC protocols for whole-brain and whole-body clearing and imaging. *Nat Protoc*. 2015;10:1709–1727.
37. Kubota SI, Takahashi K, Nishida J, et al. Whole-body profiling of cancer metastasis with single-cell resolution. *Cell Rep*. 2017;20:236–250.
38. Tainaka K, Murakami TC, Susaki EA, et al. Chemical landscape for tissue clearing based on hydrophilic reagents. *Cell Rep*. 2018;24:2196–2210.e2199.